HHS Public Access

Author manuscript

Dev Biol. Author manuscript; available in PMC 2016 August 15.

Published in final edited form as:

Dev Biol. 2015 August 15; 404(2): 76–87. doi:10.1016/j.ydbio.2015.05.018.

Rectification of muscle and nerve deficits in paralyzed ryanodine receptor type 1 mutant embryos

M. Gartz Hanson[*] and **Lee A. Niswander**

Department of Pediatrics University of Colorado School of Medicine and Children's Hospital Colorado, Aurora, CO 80045, United States

Abstract

Locomotion and respiration require motor axon connectivity and activation of the neuromuscular junction (NMJ). Through a forward genetic screen for muscle weakness, we recently reported an allele of ryanodine receptor type 1 (*Ryr1*^{AG}). Here we reveal a role for functional RyR1 during acetylcholine receptor (AChR) cluster formation and embryonic synaptic transmission. *Ryr1*^{AG} homozygous embryos are non-motile. Motor axons extend past AChR clusters and enlarged AChR clusters are found under fasciculated nerves. Using physiological and pharmacological methods, we show that contractility can be resumed through the masking of a potassium leak, and evoked vesicular release can be resumed *via* bypassing the defect in RyR1 induced calcium release. Moreover, we show the involvement of ryanodine receptors in presynaptic release at the NMJ. This data provides evidence of a role for RyR1 on both the pre- and postsynaptic sides of the NMJ.

Keywords

Diaphragm; Motoneuron; Acetylcholine; Excitation; contraction coupling

1. Introduction

The mechanisms that establish and maintain axon outgrowth and synaptic function during embryonic development are crucial for proper locomotion (Busetto et al., 2003; Hanson and Landmesser, 2004, 2006; Krull, 2010; Sanes and Lichtman, 1999, 2001) A key component of the locomotor circuit is the neuromuscular junction (NMJ), which is formed and refined by signaling between the motoneuron and the muscle (Sanes and Lichtman, 2001). Therefore, defects in pre- and postsynaptic signaling at the NMJ may have detrimental effects on neonatal survival.

Presynaptic vesicular release of acetylcholine (ACh) by motor nerve terminals leads to focal depolarization of the post-synaptic apparatus. A large action potential sweeps through the muscle fiber to induce global depolarization and muscle contraction. Contractions in muscle transpire through the opening of a muscle-specific voltage gated channel, dihydropyridine

[*]Corresponding author: Fax: +1 303 724 3792. martin.hanson@ucdenver.edu (M. Gartz Hanson).

Disclosures

The authors have declared that no conflict of interest exists.

receptor (L-type calcium channel DHPR; Cacna1s, CaV1.1, (Franzini-Armstrong and Jorgensen, 1994)), which stimulates ryanodine receptor type 1 (RyR1) in the sarcoplasmic reticulum to flood the myoplasm with calcium. The increased calcium initiates contraction in the skeletal muscle (Numa et al., 1990). These events constitute excitation–contraction coupling (E–C coupling).

Transgenic studies have shown that skeletal muscle DHPR acts independently of E–C coupling to establish muscle prepatterning of AChR clusters, AChR cluster size, the frequency of ACh dependent depolarization, and expression of MuSK (Chen et al., 2011). Moreover, RyR1 is required for establishing muscle prepatterning of AChR clusters and proper axon outgrowth (Hanson and Niswander, 2014). However, the requirement for functional RyR1-DHPR complex in determining AChR cluster size, the frequency of ACh-dependent depolarization, and expression of MuSK is less clear.

The family of ryanodine receptors is required for proper Ca^{2+} release from the sarcoplasmic reticulum in skeletal muscle (RyR1 and RyR3) and heart (RyR2) (Coussin et al., 2000; Giannini et al., 1995; Nakai et al., 1990; Otsu et al., 1990; Takeshima et al., 1989; Zorzato et al., 1990). Mice that lack either *Ryr1* or *Ryr2* die at birth (Takeshima et al., 1994, 1998), whereas mice that lack *Ryr3* are viable (Takeshima et al., 1996), but have deficiencies in synaptic plasticity and locomotion (Futatsugi et al., 1999). Embryonic rat spinal cord and cultured rat motoneurons express RyR1, RyR2, and RyR3 (Dayanithi et al., 2006) and this family of intracellular receptors is required for Ca^{2+} release from the endoplasmic reticulum of neurons (Fill and Copello, 2002). Therefore, RyRs regulate muscle Ca^{2+} release and may be involved in release of Ca^{2+} in the presynaptic terminal that results in release of transmitter.

Here we explore the function of RyR1 as it pertains to mechanisms of motoneuron axon extension, AChR cluster distribution, and presynaptic transmitter release. Mouse embryos that are homozygous for a point mutation in *Ryr1* ($Ryr1^{AG}$) have defects in axon extension, abnormally narrow distribution of AChR clusters and increased AChR cluster size. The $Ryr1^{AG/AG}$ embryonic muscle has a greater change in internal potassium levels and muscle paralysis but, by inhibiting the potassium leak, the muscle can be stimulated to undergo contractions. In addition, we use this mouse model to uncover a pre-synaptic role of ryanodine receptors at the mouse neuromuscular junction. Overall, these data illustrate that RyRs are involved in vesicular release at the NMJ, RyR1 is required for proper release of transmitter at the neuromuscular junction, and postsynaptic RyR1 is required for the size and distribution of AChR clusters.

2. Material and methods

2.1 Forward genetic screen and mouse strains

ENU mutagenesis was performed as described (Kasarskis et al., 1998) on males of C57BL/6J background and then outcrossed onto 129S1/Svlmj background to score at embryonic day 18.5 for recessive mutations that affect embryonic locomotion. The forward genetic screen and identification of the $Ryr1^{AG}$ mutation is described in Hanson et al. (2015). This allele is named $RyR1^{m1Nisw}$ but here we will refer to it as $Ryr1^{AG}$. $Ryr1^{-/-}$ is the

dyspedic null mutation (*Ryr1*^{tm1TAlle} allele generated by Richard Allen (Buck et al., 1997)). To examine axon guidance errors in limb muscles, *Ryr1*$^{AG/+}$ mice were crossed with B6.Cg-Tg(Hlxb9-GFP)1Tmj/J (Jackson laboratory, Maine) stated as *Hlxb9-GFP* then outcrossed 6 generations in 129S1/Svlmj background. For the locomotion screen, E18.5 embryos were dissected from timed pregnant dams and placed in room temperature oxygenated mouse Tyrode's solution. To induce limb movement, forelimb and hindlimb footpads were pinched with tweezers to induce paw retraction and cross-extensor reflexes. Touching the forceps to the dorsal rib cage scored s-shaped movements in axial muscles. Touching the forceps to the nose scored neck extension reflex. Touch assay was performed on each embryo in the litter and the genotype of all embryos was determined.

2.2 Calcium transient measurements

Primary myoblasts isolated from E18.5 embryonic muscle were differentiated and then loaded with the fluorescent Ca^{2+} indicator Fluo-3 (Life Technologies, Grand Island, NY) injected by whole-cell configuration at a final concentration of 200 μM. Following loading, Fluo-3 dye was allowed to diffuse within the cell interior for 5 min. The total change in fluorescence ($\Delta F/F$) was determined from the change in peak fluorescence from initial baseline during stimulation, where F was the fluorescence immediately before the test pulse minus the measured average background (non–Fluo-3) fluorescence before dye injection. The average values of fluorescence change (ΔF) for each test potential (V) were fitted according to: $(\Delta F)=(\Delta F)_{max}/\{1+\exp[(V_F - V)/k_F]\}$, where $(\Delta F)_{max}$ =1093 au, V_F = −1.4 mV and k_F =5.5 mV. Fluorescence emission was measured by fluorometer (Biomedical Instrumentation Group, University of Pennsylvania, Philadelphia, PA). Kurt Beam and Roger Bannister provided *Ryr1*-YFP cDNA and performed these experiments.

2.3 [K$^+$]i/PBFI measurements

For [K+]i measurements, E18.5 diaphragm muscle was mechanically scraped of membrane bordering the muscle and affixed to glass bottom culture dishes (MatTeK) with Vetbond (3 M, St. Paul, MN). The ratiometric cell-permeant potassium indicator PBFI–AM (5 μM; Life Technologies, Grand Island, NY) together with 0.2% Pluronic F-127 for enhanced dye loading was applied to the diaphragm muscle for 30 min in Ringers Solution (3 mM K^+). After loading, muscles were washed for 30 min to remove excess dye and to allow deesterification of the AM dye. Data was collected from greater than 10 fibers per muscle with 4 muscles per condition. Muscles were analyzed at 33 °C using the 340/380 filters on Zeiss Axio Observer Z1 with Photometrics CoolSNAP HQ2 camera for wide-field imaging. The filtered 340 and 380 intensities were analysized per second and the ratiometric intensity for the fibers were plotted. To calibrate intracellular potassium concentrations, ratiometric PBFI intensities were fitted to the intensities at different K^+ concentrations with the addition of 10 μM gramicidin in extracellular solutions and using the intensity of ~10 fibers of interest per muscle in >3 muscles from each condition. Calibration solutions were prepared with appropriate volumes of a high [K^+] solution with potassium gluconate.

2.4 ATP content

E18.5 limb skeletal muscles were assayed immediately after homogenization using buffer described in Hanson et al. (2015) to determine ATP content with a luciferin–luciferase based bioluminescence assay. The methodology of the ATP determination kit is provided in the experimental protocol by Molecular Probes (A-22066, Eugene, OR, USA). In order to determine ATP content, freshly extracted homogenate was added to a cuvette containing reaction buffer, D-luciferin, luciferase and DTT and placed in a Sirius luminometer v.2.2 (Berthold Detection Systems). Known concentrations of ATP standards were used to establish a standard curve.

2.5 Electrode recordings

Sharp electrode recordings were performed as described (Hanson et al., 2014; Plomp et al., 1992). E18.5 diaphragms were dissected and kept at room temperature in Normal Ringers solution. Diaphragm muscle fibers were impaled with a glass capillary microelectrode (30 MΩ resistance) made using a P-97 microelectrode puller (Sutter Instruments, Novata, CA) and filled with 3 M KCl (Brown et al., 2008). Evoked responses were elicited by a 0.2-ms maximal stimulus applied to the phrenic nerve using a suction electrode and pulse generator (STG 1002, ALA Scientific Instruments, Farmingdale, NY). Evoked and miniature endplate potentials (MEPP) were recorded using an Axoclamp-2A amplifier (Molecular Devices, Sunnyvale, CA) and DigiData 1322A (Molecular Devices). Muscle fiber membrane potentials were adjusted to $E_m = -70$ mV under current clamp. Data was extracted and analyzed with Axoscope 10 software (Molecular Devices).

For EMG recordings and analysis of muscle contractions, explanted diaphragm muscle (Hanson and Niswander, 2014) was warmed to 30 °C and continually supplied with oxygenated Tyrode's solution (3.0 mM KCl). EMG muscle recordings were made using fine-tip suction electrodes pulled from polyethylene tubing (PE-190; Clay Adams, NJ) and recorded *via* amplifiers (AI 401 amplifier connected with Digidata 1322a, Molecular Devices) directly on the computer with Axoscope 10 (Molecular Devices). Significance of data was evaluated by Student's *t*-test, which determined the *P* value (Excel 2008). A *P* value below 0.05 was considered significant. E18.5 diaphragm preparations were treated with pharmacological reagents by addition of drugs to the bath at the indicated concentrations. For contractile studies, a stimulation electrode was placed onto the diaphragm. Evoked response was elicited by a 0.2-ms maximal stimulus compared to locomotor normal littermates within bath. A contractile movement was scored as a 0 if no contraction transpired after stimulation and 1 if contraction was recorded either through EMG recording or a visual confirmation. Drugs were bath applied for a minimum of 1 min before examination of contractility.

2.6 Electron microscopy

Diaphragm muscles of E18.5 embryos were fixed with 2.0% glutaraldehyde in 0.1 M cacodylate buffer (pH 7.2) at 37 °C. The central region of muscle was dissected to focus on the predominant region of AChR clusters, followed by a secondary post-fixation in 2% osmium tetroxide and 1.5% potassium ferrocyanide in 0.1 M cacodylate (Sigma-Aldrich, St. Louis, MO) buffer for 1 h at room temperature. Samples were dehydrated through an

ethanol series (50, 70, 90, 95 and 100% ETOH) and embedded in Epon/ Araldite resin polymerized overnight at 60 °C. Ultrathin sections were cut, placed on copper mesh grids and double contrasted with 2% aqueous uranyl acetate and Reynold's lead citrate. Grids were imaged using a FEI Technai G2 BioTwin transmission electron microscope (FEI, Hillsboro, OR). Vesicle size and number were calculated using ImageJ.

2.7 In situ hybridization

Whole mount *in situ* hybridization was carried out as previously described (Lin et al., 2001). E15.5 embryos were dissected in oxygenated Tyrode's Solution and pinned to a dish with a layer of Sylgard (184, Dow Corning) and the skin removed to expose the ribcage. A portion of the ribcage surrounding the diaphragm (last 5–8 caudal ribs) was removed from the embryo with small scissors and placed rostrally on another 100 mM Sylgard coated dish with the ribcage slightly stretched and pinned down using insect pins. Diaphragms were fixed in freshly prepared 4% PFA in 0.1 M phosphate buffer at 4 °C overnight and then dehydrated through a series of methanol solutions (25, 50, 75 and 100%). Hybridization was carried out at 70 °C overnight in hybridization buffer containing 50% formamide (Sigma), 1.3 × SSC, 50 μg/ml yeast tRNA, 0.2% Tween-20, and 1% Triton X-100 (Sigma), using digoxigenin-labeled *Lrp4* or *MuSK* riboprobes. Diaphragms were washed with TBS containing 1% Tween-20, blocked with 5% goat serum in dilution buffer, and incubated with alkaline phosphatase conjugated anti-digoxigenin antibody (1:1000, Boehringer Mannheim GMBH, Indianapolis, IN) overnight at 4 °C, and hybridization signals were detected with a staining solution containing 100 mM Tris (pH 9.5), 0.4 mg/ml nitro blue tetrazolium chloride (NBT), 0.19 mg/ml 5-Bromo-4-chloro-3-indolyl phosphate (BCIP), 100 mM NaCl and 50 mM $MgCl_2$ (Sigma).

2.8 Quantitative RT-PCR

RNA was extracted from spinal cord using Trizol® followed by DNaseI digestion and clean-up (Qiagen RNAeasy Minikit, Qiagen, Valencia, CA) and reverse transcribed using random hexamer primers and SuperScript III Reverse Transcriptase (Life Technologies) and amplified using TaqMan Universal PCR Master Mix (Life Technologies). Quantitative PCR was performed on a Roche LightCycler 480 Real-Time PCR System. Calculations were performed by a relative standard curve method. Probes for target genes were from TaqMan Assay-on-Demand kits (Life Technologies). Samples were adjusted for total RNA content by GAPDH in muscles of control embryos.

2.9 Immunohistochemistry

Diaphragms were dissected and pinned to sylgard dish in 4% paraformaldehyde for 10 min then permeabilized with 0.2% Triton/ PBS for 30 min. Non-specific reactivity was blocked with 2% BSA/ PBS for 2 h. When diaphragms were exposed to α-BTX conjugated Alexa 555 (1:500) alone, no permeabilization was performed to allow detection of AChRs at the membrane. Primary monoclonal antibody for all RyRs (34C, 1:20; Airey et al., 1990) was applied overnight at room temperature. Primary antibodies for neurofilament (1:100; Sigma) and synaptophysin (1:200; DSHB) were applied overnight at 4 °C. Secondary antibodies

(Alexa Fluor 488-conjugated donkey anti-mouse, Alexa Fluor 568-conjugated goat anti-mouse IgG, 1:500, Life Technologies, #A11031) were applied for 1 h.

2.10 Confocal microscopy

Immunostained samples were examined by confocal laser scanning microscopy using a Zeiss LSM 510. For diaphragms, an area of 1 mm^2 was selected from the field of view (×10). Alexa-Fluor 568 was excited at 543-nm by a HeNe laser line (1 mW maximum output, operated at 100%), directed *via* a 488/543 nm dual dichroic mirror. Emitted fluorescence was directed to a photomultiplier with a 560-nm long-pass filter. Confocal fluorescence intensity data were recorded as the average of four line scans per pixel and digitized at 8-bits, with photomultiplier gain adjusted such that maximum pixel intensities were <70% saturated.

2.11 Quantification

The ventral quadrant of the diaphragm shows a high degree of reproducibility in axon branching, AChR cluster number and distribution. Drawing a line between the most distal α-bungarotoxin positive AChR clusters and measuring the distance in ~10 μm intervals on each side of the central branch nerve in the ventral diaphragm quadrant quantified AChR cluster region. To determine the percent of the region occupied by AChR clusters, the distance to the distal edges of the diaphragm and the region of α-bungarotoxin labeled AChR clusters was measured in 100 μm increments. Percentage of AChR clusters was quantified using compressed z-stack images. Each condition was performed in at least 5 diaphragms for each condition. AChR cluster number was quantified on z-stack images of entire muscle by dividing the ventral quadrant into 0.1 mm bins from central branch in ventral quadrant outlined by purple boxes in Fig. 3A and B. The Zen 2009 software (Zeiss, Germany) was used to calculate the size of the AChR clusters.

2.12 Statistical analysis

The unpaired two-tailed Student's *t*-test was used to examine statistical differences. Data in the manuscript are represented as mean ± SEM unless otherwise indicated. $p<0.05$ was considered significant.

2.13 Study approval

All experiments were conducted in accordance with the protocols described in the Guide for the Care and Use of Laboratory Animals (NIH, Revised 2011).

3. Results

3.1 RyR1^{AG} protein is expressed but the mutation causes a non-motile embryonic phenotype

Following N-ethyl-N-nitrosourea (ENU) chemical mutagenesis and a multi-generation cross to identify recessive mutations, the *Ryr1*^{AG} line was identified by muscle weakness (Hanson et al., 2015). The ENU-induced point mutation creates an E4242G change in exon 93, outside of the channel region of RyR1. To study the phenotype in mice homozygous for the *Ryr1*^{AG} allele, *Ryr1*$^{AG/+}$ mice were crossed. At embryonic day 18.5 (E18.5), *Ryr1*$^{AG/AG}$

homozygous mutant embryos displayed kyphosis (hunchback), carpoptosis (wrist drop), were non-motile during the locomotion screen (see methods) and died at birth (Fig. 1A). Gene identification was confirmed by a lack of complementation in trans-heterozygous embryos for our allele and *RyR1* null allele and the $Ryr1^{AG/AG}$ phenotype was similar to $RyR1^{-/-}$ embryos (Fig. 1A). Next, *Ryr1* RNA levels in the $Ryr1^{AG/AG}$ mouse embryonic spinal cord were determined at E14.5 and E18.5 and showed no significant difference compared to wildtype age matched embryos (n=4; Fig. S1). RyR1 is the predominant family member in muscle and using a pan RyR antibody we observed RyR immunoreactivity in puncta-like patterns in the tetrads of muscle fibers in both $Ryr1^{AG/+}$ and $Ryr1^{AG/AG}$ muscle (Fig. 1B and C). In myotube cultures, locomotor normal and $Ryr1^{AG/AG}$ myotubes have detectable RyR protein expression (Fig. 1D and F), whereas no protein is detected in *Ryr1* null myotubes (Fig. 1E and G is antibody control). These data indicate that the $Ryr1^{AG}$ allele has no apparent effect on *Ryr* mRNA or protein expression in the spinal cord or muscle.

3.2 Defects in calcium dynamics in $Ryr1^{AG/AG}$ mice

RyR1 functions as a muscle isotype of ryanodine receptors that is mechanically activated by the dihydropyridine receptor to allow Ca^{2+} release from the sarcoplasmic reticulum (SR), thus evoking E–C coupling (Fill and Copello, 2002; Takeshima et al., 1994). To determine whether $Ryr1^{AG}$ mutant protein affects calcium release, myotube cultures were used, as RyR1 function has been well studied in this system (Bannister and Beam, 2009; Fill and Copello, 2002). Whole-cell clamping in combination with fluorescent Ca^{2+} indicator (Bannister et al., 2008) showed that, unlike normal myotubes, $Ryr1^{AG/AG}$ myotubes failed to release Ca^{2+} from the SR in response to change in membrane potential (Fig. 2A–C $Ryr1^{+/+}$ light gray circles and $Ryr1^{AG/AG}$ dark gray circles). Moreover, $Ryr1^{AG/AG}$ myotubes failed to contract in response to electrical stimulation but electrically-evoked contractions could be rescued by expression of YFP-tagged wildtype RyR1 in $Ryr1^{AG/AG}$ myotubes (Fig. 2D), further evidence that the *RyR1* mutation is causative of the phenotype. Addition of the RyR1 agonist, 4-chloro-*m*-cresol (4-C*m*C; 0.5 mM), produced substantial Ca^{2+} release in both normal and $Ryr1^{AG/AG}$ myotubes (peak $\Delta F/F$ of 1.4±0.1; n=5 *vs*. 1.2±0.1; n=3, respectively; p>0.05; Fig. 2E and F), compared to $Ryr1^{-/-}$ myotubes ($\Delta F/F$ 0.1±0.0; n=6; Fig. 2F). These results indicate that $RyR1^{AG/AG}$ protein is present in myotubes and can release SR Ca^{2+} stores with the help of an agonist to RyR. However, the rate of SR Ca^{2+} release in response to 4-C*m*C was much slower in $Ryr1^{AG/AG}$ myotubes than in normal myotubes ($t_{1/2}$act =6.5±2.4 *vs*. 2.2±0.6 s, respectively; p<0.01; Fig. 2E). This suggests a functional disruption of the $RyR1^{AG/AG}$ channel is responsible for the lack of evoked release of calcium from internal stores.

3.3 Inhibition of potassium leak in $Ryr1^{AG/AG}$ muscles

Our recent studies of adult $Ryr1^{AG/+}$ mice demonstrated a myopathy with core-like structures and mechanistically this was related to a potassium leak (Hanson et al., 2015). The K^+ leak could be masked either by raising external K^+ or by inhibiting K_{ATP} channel outward current, which rescued the myopathy in $Ryr1^{AG/+}$ muscles. To determine whether a similar K^+ leak underlies the non-motile phenotype in $Ryr1^{AG/AG}$ embryos, we first assessed K^+ homeostasis in $Ryr1^{AG/AG}$ diaphragms using the potassium indicator PBFI–AM (see Section 2) in combination with ratiometric potassium imaging of muscle fibers. Experiments

using wildtype diaphragms in normal Ringers solution (3 mM K^+) showed that intracellular K^+ concentration was 144±7 mM (*n*=33 fibers from 4 diaphragms; Fig. 3A and C). *Ryr1*$^{-/-}$ null diaphragms exhibited intracellular concentration similar to wild-type diaphragms (139±11 mM; *n*=30 fibers from 4 diaphragms, Fig. 3C). However, *Ryr1*$^{AG/AG}$ diaphragms showed lower intracellular K^+ concentrations of 85±15 mM (*n*=41 fibers from 5 diaphragms; $p<0.001$; Fig. 3B and C), suggestive of a potassium leak.

In adult *Ryr1*$^{AG/+}$ muscles, the mutant *RyR1* inhibits Ca^{2+} release, which results in decreased ATP content and dysregulation of genes and proteins involved in potassium homeostasis (Hanson et al., 2015). ATP content in *Ryr1*$^{AG/AG}$ diaphragm muscle was significantly decreased compared to wildtype (21±4 nmol/mg *Ryr1*$^{AG/AG}$ muscles versus 35±6 in wildtype; *n*=4 per mouse line; Fig. 3D). *Ryr1*$^{-/-}$ diaphragm muscles had ATP content (31±4 nmol/mg *Ryr1*$^{-/-}$ muscle; *n*=4) similar to wildtype (Fig. 3D), suggesting that Ca^{2+} internal release persist in *Ryr1*$^{-/-}$ muscle. This data suggests that RyR1$^{AG/AG}$ protein affects ATP levels which may suggest that potassium homeostasis is also affected in these diaphragms. As in *Ryr1*$^{AG/+}$ soleus muscles (Hanson et al., 2015), *Ryr1*$^{AG/AG}$ diaphragm fibers showed a greater change in K^+ fluorescent ratio intensity over the course of testing suggesting more fluctuations in K^+ ion permeability compared to wildtype diaphragms (Fig. 3E and F; *n*=41 fibers in 5 *Ryr1*$^{AG/AG}$ diaphragms and *n*=33 fibers in 4 wildtype diaphragms and *n*=30 fibers in *Ryr1*$^{-/-}$ diaphragms). The K^+ leak could be amplified in all muscles by depleting the muscle of extra-cellular K^+, however the change in PBFI intensity was significantly greater in *Ryr1*$^{AG/AG}$ diaphragms compared to wildtype and *Ryr1*$^{-/-}$ diaphragms (Fig. 3E and F). The addition of 6 mM KCl or glibenclamide (2 μM) inhibited K^+ loss and significantly increased intracellular K^+ intensity of the muscle fibers of *Ryr1*$^{AG/AG}$ diaphragms compared to wildtype and *Ryr1*$^{-/-}$ diaphragms (Fig. 3E and F). These data suggest that *Ryr1*$^{AG/AG}$ diaphragms have decreased intracellular K^+, decreased ATP content and greater fluctuations in internalized K^+.

3.4 Resumption of contractility in Ryr1$^{AG/AG}$ muscles

The inhibition of the K^+ leak by 6 mM KCl might increase intracellular K^+ and this may be sufficient to initiate a contraction. Using electromyography recordings (EMG) we examined muscle contractions in whole diaphragm muscle *in vitro* upon direct muscle stimulation. In 3 mM KCl Ringers solution, stimulation of diaphragms initiated whole muscle contractions in wildtype diaphragms but not in *Ryr1*$^{AG/AG}$ or *Ryr1*$^{-/-}$ diaphragms (Fig. 3G and H). Increasing KCl from 3 mM to 6 mM together with electrical stimulation of the diaphragm induced bursts of electrical activity in the EMG recordings and whole muscle contractions in wildtype and *Ryr1*$^{AG/AG}$ muscle but not *Ryr1* null muscle (Fig. 3G and H). The potassium leak in adult *Ryr1*$^{AG/+}$ muscle can be masked through inhibiting K_{ATP} channels with glibenclamide (2 μM; Hanson et al., 2015). The addition of glibenclamide to the bath induced contractions in *Ryr1*$^{AG/AG}$ but not *Ryr1*$^{-/-}$ muscle (Fig. 3H). These data provide *in vitro* evidence that homozygous RyR1^{AG} channels have the ability to be functional active, but the channel might be forced into an inactive state due to a potassium leak.

If the RyR1^{AG} channel is in an inactive state due to defects in membrane excitability, the pharmacological activation of the voltage-dependent DHPR might force RyR1^{AG} into an

active state, allowing release of stored Ca^{2+} to instigate a contraction. To examine the ability of the DHPR channel to engage excitation–contraction coupling, Bay K8644 (100 nM), an agonist to the channel portion of DHPR, was applied to *Ryr1*$^{AG/AG}$ diaphragm muscle. Indeed, Bay K8644 addition could induce muscle contractions, whereas no contractions occurred in *Ryr1* null diaphragm muscle (Fig. 3H). This indicates that orthograde DHPR-RyR1 signaling can be elicited in *Ryr1*$^{AG/AG}$ muscle.

3.5 RyR1 signaling participates in axon extension and postsynaptic AChR cluster distribution

Two mouse models that disrupt E–C coupling due to lack of evoked calcium release from internal stores-targeted deletion of β1 subunit of DHPR *(Cacnb1*^{null}) (Chen et al., 2011) and deletion of Stac3 (Nelson et al., 2013), which disrupts the voltage activation of DHPR and affects RyR1 calcium release, show increased axon branching and extension and broad disorganization of AChR clusters throughout the muscle. In contrast, loss of RyR1 function causes regionalization of AChR clusters around large nerve bundles (Hanson and Niswander, 2014). To determine the effect of the *Ryr1*$^{AG/AG}$ allele, we examined AChR cluster distribution and axon extension in E18.5 *Ryr1*$^{AG/AG}$ muscle. In normal E18.5 diaphragm, postsynaptic AChR clusters are centralized and distributed under the branched axons (Fig. 4A and inset shown in Fig. 4C; labeled with α-bungarotoxin [αBTX, red], neurofilament and synaptophysin [green]). In *Ryr1*$^{AG/AG}$ mutant diaphragm, motor axons were present and there were similar numbers of AChR clusters in *Ryr1*$^{AG/AG}$ compared to *RyR1*$^{AG/+}$ (Fig. 4A, B and E). However, *Ryr1*$^{AG/AG}$ diaphragms exhibited a narrowed region of AChR cluster distribution showing an ~50% reduction in width in the region of the AChR clusters compared to normal littermates (Fig. 4C, D and F). Furthermore, the axons extended past these AChR clusters resulting in longer axons in *Ryr1*$^{AG/AG}$ compared to *Ryr1*$^{AG/+}$ diaphragms (Fig. 4D and G). In other muscles of *Ryr1*$^{AG/AG}$ embryos, axons extended past narrowed AChR clusters (Fig. S2 shows gluteus maximus and vastus lateralis muscles). In *Ryr1* null diaphragms, axons also extended past the AChR clusters and the AChR cluster region was narrowed (Fig. 4E–G). Similar to *RyR1*$^{-/-}$ E15.5 diaphragms that lack phrenic nerves (Hanson and Niswander, 2014), MuSK and Lrp4, proteins important in postsynaptic AChR formation, axon outgrowth and synapse stability, show narrowed RNA expression patterns at E14.5 and E18.5 in *Ryr1*$^{AG/AG}$ diaphragms compared to normal (Fig. 4H–O). This is in contrast to *Cacnb1*^{null} embryos in which *Musk* is over-expressed throughout the diaphragm and AChR clusters are distributed throughout the diaphragm (Chen et al., 2011). This data suggests significant functional differences resulting from mutations to either the DHPR or RyR1.

3.6 RyR1 restricts size of AChR clusters

Recently, our examination of E18.5 *Ryr1*$^{-/-}$ diaphragms provided evidence that the majority of AChR clusters do not distribute with the overextended axons (Hanson and Niswander, 2014). At E18.5, individual synapses appeared to be larger in *Ryr1*$^{AG/AG}$ diaphragm muscle than in the age-matched control embryos (Fig. 5A, B and D), while *Ryr1*$^{-/-}$ AChR clusters varied in size and shape with nonfluorescent regions within the middle and to the sides of the disk (Fig. 5C and D). Measurements of individual AChR clusters showed an ~50% increase in size of AChR clusters in *Ryr1*$^{AG/AG}$ muscles compared with normal controls

(Fig. 5D). This suggests that functional RyR1 channels in muscle or nerve may regulate AChR cluster size and distribution during NMJ development.

3.7 Enhanced spontaneous transmitter release on Ryr1$^{AG/AG}$ muscle

In order to examine the presynaptic side of the NMJ, an electron microscopy analyzes was performed on E18.5 mouse diaphragm muscle/phrenic nerve region. In *Ryr1*$^{AG/AG}$ diaphragms (*n*=15), the presynaptic nerve terminals contained increased numbers of vesicles compared to *Ryr1*$^{AG/+}$ AChR clusters (265±38 in *Ryr1*$^{AG/AG}$ compared to 165±25 in *Ryr1*$^{AG/+}$ per terminal; *n*=20 sections used per genetic background) with decreased size (32 nm^2±11 in *Ryr1*$^{AG/AG}$ (*n*=621) compared to 52±18 in *Ryr1*$^{AG/+}$ (*n*=605)), while the basal lamina was well defined (Fig. 6A–D). In order to determine whether the NMJ in the *Ryr1*$^{AG/AG}$ embryos were functional, electrophysiological analysis was performed on E18.5 diaphragm muscle (Fig. 6E–I). Spontaneous neuromuscular synaptic activity, as measured by miniature endplate potential (mEPP) frequency in the absence of stimulation (events per minute), was increased more than 80-fold in *Ryr1*$^{AG/AG}$ muscles (69.11±16.79, *n*=21 cells, *n*=6 embryos, 8915 total events in 129 min) compared with controls (0.79±0.21, *n*=25 cells, *n*=5 embryos, 113 total events in 143 min; $p<0.005$; Fig. 6. E, F and H). In *RyR1*$^{-/-}$ diaphragm muscle mEPP were modestly increased compared to controls (5.92±2.21, *n*=18 cells, *n*=5 embryos, 959 total events in 162 min; Fig. 6G and H). Examination of the magnitude of mEPP show variability in the amplitudes in *Ryr1*$^{AG/AG}$ muscles, but no significant increase in size (2.38±0.81 mV, *n*=21 cells and 6 embryos) compared with controls (1.97±0.22 mV, *n*=25 cells and 5 embryos; $p<0.05$; Fig. 5I) or *Ryr1*$^{-/-}$ muscle (2.08±0.62 mV, *n*=19 cells and 4 embryos; $p<0.05$).

CACNB1/DHPR (Chen et al., 2011) and STAC3 (Nelson et al., 2013) increase the incidence of mEPPs in age-matched diaphragm muscle, suggesting that signaling in muscle affects the frequency of spontaneous ACh release onto the post-synaptic endplate. To determine whether ryanodine receptors in the nerve regulate mEPP frequency, mEPPs were examined in E18.5 *Ryr1*$^{-/-}$ diaphragms. The application of 4-C*m*C (0.5 mM; to activate endogenous presynaptic RyR2 without activating pre- and post-synaptic RyR3 (Choisy et al., 1999; Fessenden et al., 2000)) to the bath increased the incidence of mEPPs in *Ryr1*$^{-/-}$ muscle (29.87±10.29, *n*=20 cells, *n*=5 embryos, 3734 total events in 125 min; Fig. 6J). Bath application of caffeine (10 mM; agonist for all three RyRs) showed an even greater incidence of mEPPS in *Ryr1*$^{-/-}$ muscle, suggesting that both RyR2 and RyR3 mediated Ca^{2+} release can affect mEPP frequency (43.76±12.77, *n*=19 cells, *n*=5 embryos, 5252 total events in 120 min; Fig. 6J). Moreover, these data suggest that RyR2 channels are in the pre-synaptic apparatus and involved in NMJ transmission. To determine whether genetic alteration of RyR1 function can change the amount of RNA produced from the three *Ryr* family member genes, we performed quantitative RT PCR on the ventral spinal cords of *Ryr1*$^{-/-}$, *Ryr1*$^{AG/AG}$ and *Ryr1*$^{+/+}$ E18.5 embryos. Under these conditions, no significant differences were found in the level of *Ryr2* or *Ryr3* RNA (Fig. 6K), suggesting the RyR2 effect on mEPP frequency is not due to an alteration in *Ryr2* transcript in the spinal cord.

3.8 Lack of evoked endplate potentials in Ryr1$^{AG/AG}$ diaphragms

To further examine the motor axon electrophysiology of the NMJ, evoked endplate potentials (eEPPs) were induced through phrenic nerve stimulation. Amplitudes of eEPPs were similar between control (33.25±5.25 mV, *n*=23 cells and 4 embryos; Fig. 7A) and *Ryr1*$^{-/-}$ muscles (26.75±9.22 mV, *n*=27 cells and 4 embryos; Fig. 7C) in response to electrical stimulation of the nerve. Notably, in *Ryr1*$^{AG/AG}$ diaphragm muscle, stimulation did not induce eEPPs (*n*=35 cells and 5 embryos; Fig. 7B compared to locomotor normal littermate in Fig. 7A). The lack of evoked release in *Ryr1*$^{AG/AG}$ could be due to a presynaptic defect and, if so, this would suggest a role for presynaptic RyR1 at the neuromuscular junction. The non-functioning neuronal RyR1 might compromise the production or availability of components required for vesicular release. To test this, 10 mM Ca^{2+} was bath applied and this was capable of restoring evoked potentials in *Ryr1*$^{AG/AG}$ diaphragm muscles (Fig. 8A; compared to Fig. 7B without additional Ca^{2+}). The initial application of 10 mM Ca^{2+} to the bath induced asynchronous release of transmitter which suppressed the high number of mEPPs produced in control Ca^{2+} solutions. This data suggests that the components for evoked release are present and able to function. This data suggest that the *Ryr1*$^{AG/AG}$ mutation might affect the availability of necessary Ca^{2+} to support evoked ACh release onto the muscle. To increase cytosolic Ca^{2+} levels in *Ryr1*$^{AG/AG}$ preparation, treatment with 4-C*m*C (500 μM) and phrenic nerve stimulation produced eEPPs in the muscle and increased the number of mEPPs (Fig. 8D compared to 7B, arrowheads highlight mEPPs in Fig. 8). 4-C*m*C induced evoked response in *Ryr1*$^{AG/AG}$ muscle immediately after application suggesting that presynaptic RyR (RyR1 and/or RyR2) are involved in evoked release of ACh. Moreover, depleting internally stored Ca^{2+} with bath application of thapsigargin (1 μM) temporarily restored eEPPs in *Ryr1*$^{AG/AG}$ diaphragms (Fig. 8F), suggesting the evoked release involvement of ER-like membranes on the presynaptic side of the NMJ. These data suggests that functional neuronal ryanodine receptor channels can be involved in the action potential-mediated release and spontaneous release of synaptic vesicles at the NMJ.

4. Discussion

Here we present homozygous embryonic data from a myopathic *RyR1*^{AG} mouse model that demonstrates structural and functional defects of the muscle and nerve. Of the structural defects, we first substantiate that axons extend beyond the AChR cluster region and AChR clusters become more centralized in *Ryr1*^{AG} and *Ryr1*$^{-/-}$ muscle. Second, we show that AChR clusters in dysfunctional *Ryr1*^{AG} muscle are consistently larger than AChR clusters in wildtype and *Ryr1*$^{-/-}$ null muscle. Of the functional defects, we first describe that the homozygous RyR1^{AG} protein is present but dysfunctional in the muscle. Second, we provide evidence of a K^+ leak in *Ryr1*$^{AG/AG}$ diaphragms, and that masking of the K^+ leak induces muscle contractions in otherwise paralyzed muscle. Third, we demonstrate that unlike wildtype and *Ryr1*$^{-/-}$ NMJs, NMJs in *Ryr1*$^{AG/AG}$ lack release of Ca2+ in the presynaptic terminal that results in release of transmitter. However, supplementation by external Ca^{2+} can re-initiate evoked release. Lastly, we show that ryanodine receptors are involved in vesicular release of ACh at the NMJ. These data suggests that RyR1 contributes

to structural and functional events at the neuromuscular interface beyond the well-studied role in SR Ca^{2+} release to induce muscle contractility.

The inhibition of RyR1-dependent SR Ca^{2+} release may underscore the majority of structural changes in *Ryr1*$^{AG/AG}$ muscle. In *Cacna1s*$^{mdg/mdg}$, *Cacnb1* null and *Ryr1* null diaphragms, similarities exist in extensive axon overgrowth and AChR cluster size (Fig. 4D compared with work by Powell and work by Chen et al. (2011), Powell et al. (1984)). Our data on *Ryr1*$^{AG/AG}$ muscle and on muscle lacking *Ryr1* allows us to suggest that restriction of AChR cluster size might be dependent on RyR1 downstream signaling. However, dissimilarity exists in AChR cluster distribution between DHPR mouse models and RyR1 mouse models, AChR cluster distribution is expanded in diaphragms that lack DHPR subunits while restricted in models with abnormal RyR1 function (Fig. 4A; Chen et al., 2011; Hanson and Niswander, 2014; Powell et al., 1984). Therefore, our data and work by Chen et al. (2011) suggest an additional role for DHPR and RyR1 function beyond muscle contractility and SR Ca^{2+} release, and might play roles in axon extension, AChR distribution and AChR cluster size.

In *Ryr1*$^{AG/AG}$ muscles, we show that axons extend beyond the centralized AChR clusters and beyond *Musk* and *Lrp4* expression regions. In addition, *Musk* and *Lrp4* expression regions are narrowed and similar in extent as the centralized AChR clusters. Motor axons require proper MuSK signaling for correct placement (Kim and Burden, 2008). Moreover, Lrp4 is the receptor for agrin and component of MuSK signaling and is required for AChR cluster formation (Kim et al., 2008; Lin et al., 2001; Weatherbee et al., 2006; Yang et al., 2001). Recently, RyR1 signaling was shown to be involved in proper prepatterning of AChR clusters and axon extension (Hanson and Niswander, 2014). Therefore, our data suggest that muscle RyR1 may help the MuSK and Lrp4 signaling complex to halt axon extension. Since *Cacnb1* null (DHPR β1 null) mice show an increase in *Musk* expression (Chen et al., 2011), which contrasts with our data in *Ryr1*$^{AG/AG}$ muscles, we can conclude that muscle RyR1 may have a distinct function in axon extension separate from the role of the DHPR–RyR1 complex in SR Ca^{2+} release.

Ryanodine receptors may also have a distinct role in release of Ca^{2+} in the presynaptic terminal that results in release of transmitter at the presynaptic NMJ. Synaptic vesicles are increased at *Ryr1*$^{AG/AG}$ presynaptic nerve terminals and our pharmacological studies suggest that functional RyR1 and RyR2 are involved in release of Ca^{2+} that results in release of ACh at the NMJ and thus may also be involved in the Ca^{2+} dependent release of other factors required during NMJ development. Interactions between RyR1 and Snapin, a protein involved in peptide secretion, enhances RyR1 channel activation (Zissimopoulos et al., 2006) and stimulates peptide secretion in non-neuronal cells (Kinoshita et al., 2013). RyR channels and the vesicular release protein, SNAP25 share an overlapping binding site on Snapin, suggesting a direct link between RyR and vesicular release (Zissimopoulos et al., 2006). In *Drosophila*, dense core vesicles (DCV) are activated through CaMKII and can be modulated by ryanodine receptors (Levitan, 2008; Shakiryanova et al., 2007). In vertebrates, golgi-like apparatus release DCVs that contain agrin (Magill-Solc and McMahan, 1988). Therefore, DCV might utilize RyR dependent stores of Ca^{2+} to evoke release of agrin onto the muscle. In addition, RyR might be involved in ACh and agrin release during the

presynaptic instigation of the evoked endplate potentials, two molecules that are involved in neuronal synapse elimination and stabilization (Lin et al., 2001; Misgeld et al., 2005; Reist et al., 1992; Rimer, 2010; Wang et al., 2014; Yang et al., 2001).

Even though synapses are formed in *Ryr1*$^{AG/AG}$ diaphragms, action potential evoked SR Ca^{2+} release and muscle contractility are abolished. Muscle contractility can be rescued by masking the potassium leak from the muscle. A possible explanation for the rescue might be that signaling between the voltage sensitive DHPR channels and RyR1 channels is disrupted. DHPR channels and RyR1 channels interact through orthograde and retrograde signaling (Andronache et al., 2009; Bannister and Beam, 2009). Orthograde signaling from DHPR opens the RyR1 channel in the SR, while retrograde signaling from RyR1 controls the gating of DHPR (Bannister and Beam, 2009). The DHPR agonist Bay K8644 was able to induce contractions in *Ryr1*$^{AG/AG}$ diaphragms suggesting that orthograde signaling is unaffected. In addition, 4-C*m*C, the agonist of RyR1, can induce calcium release in homozygous *Ryr1*$^{AG/AG}$ myotubes. Therefore, Ryr1$^{AG/AG}$ channels have the ability to become activated but cannot activate under normal physiological conditions. In the future, experiments can be performed to examine the retrograde communication from Ryr1$^{AG/AG}$ to DHPR in a manner similar to Bannister and Beam (2009). Ryanodine receptors are expressed in excitable cells of vertebrates (Giannini et al., 1995). Therefore, ryanodine receptors may have functions beyond the release of internal Ca^{2+} stores and might contribute to the formation and maintenance of synaptic structures throughout the nervous system. Further study of RyR1 models might help to establish appropriate therapies for patients with myopathies.

Supplementary Material

Refer to Web version on PubMed Central for supplementary material.

Acknowledgments

The authors would like to thank Roger Bannister and Kurt Beam for generating the myotube data in Figs. 1 and 2; Danielle Marck, Bleu Knight, and Lori Bulwith for technical assistance; Dorothy Dill for TEM assistance; Rosa Moreno for critical comments on the manuscript; Steve Burden and Scott Weatherbee for probes to MuSK and Lrp4 respectively. Imaging experiments were performed in the University of Colorado Anschutz Medical Campus Advance Light Microscopy Core supported in part by Rocky Mountain Neurological Disorders Core Grant number P30NS048154 and by NIH/NCRR Colorado CTSI Grant number UL1 RR025780. Contents are the authors' sole responsibility and do not necessarily represent official NIH views.

This work was supported by Department of Pediatrics and Neuroscience Program NS 48154. MGH was supported by postdoctoral fellowships from Muscular Dystrophy Association MDA69338 and NIH F32 NS059267.

References

Airey JA, Beck CF, Murakami K, Tanksley SJ, Deerinck TJ, Ellisman MH, Sutko JL. Identification and localization of two triad junctional foot protein isoforms in mature avian fast twitch skeletal muscle. J Biol Chem. 1990; 265:14187–14194. [PubMed: 2387846]

Andronache Z, Hamilton SL, Dirksen RT, Melzer W. A retrograde signal from RyR1 alters DHP receptor inactivation and limits window Ca^{2+} release in muscle fibers of Y522S RyR1 knock-in mice. Proc Natl Acad Sci USA. 2009; 106:4531–4536. [PubMed: 19246389]

Bannister RA, Beam KG. Ryanodine modification of RyR1 retrogradely affects L-type Ca(2+) channel gating in skeletal muscle. J Muscle Res Cell Motil. 2009; 30:217–223. [PubMed: 19802526]

Bannister RA, Colecraft HM, Beam KG. Rem inhibits skeletal muscle EC coupling by reducing the number of functional L-type Ca^{2+} channels. Biophys J. 2008; 94:2631–2638. [PubMed: 18192376]

Brown AL, Johnson BE, Goodman MB. Making patch-pipettes and sharp electrodes with a programmable puller. J Vis Exp. 2008 Oct 8.(20) pii: 939.

Buck ED, Nguyen HT, Pessah IN, Allen PD. Dyspedic mouse skeletal muscle expresses major elements of the triadic junction but lacks detectable ryanodine receptor protein and function. J Biol Chem. 1997; 272:7360–7367. [PubMed: 9054435]

Busetto G, Buffelli M, Cangiano L, Cangiano A. Effects of evoked and spontaneous motoneuronal firing on synapse competition and elimination in skeletal muscle. J Neurocytol. 2003; 32:795–802. [PubMed: 15034268]

Chen F, Liu Y, Sugiura Y, Allen PD, Gregg RG, Lin W. Neuromuscular synaptic patterning requires the function of skeletal muscle dihydropyridine receptors. Nat Neurosci. 2011; 14:570–577. [PubMed: 21441923]

Choisy S, Huchet-Cadiou C, Leoty C. Sarcoplasmic reticulum Ca(2+) release by 4-chloro-m-cresol (4-CmC) in intact and chemically skinned ferret cardiac ventricular fibers. J Pharmacol Exp Ther. 1999; 290:578–586. [PubMed: 10411565]

Coussin F, Macrez N, Morel JL, Mironneau J. Requirement of ryanodine receptor subtypes 1 and 2 for Ca(2+)-induced Ca(2+) release in vascular myocytes. J Biol Chem. 2000; 275:9596–9603. [PubMed: 10734110]

Dayanithi G, Mechaly I, Viero C, Aptel H, Alphandery S, Puech S, Bancel F, Valmier J. Intracellular Ca^{2+} regulation in rat motoneurons during development. Cell Calcium. 2006; 39:237–246. [PubMed: 16324742]

Fessenden JD, Wang Y, Moore RA, Chen SR, Allen PD, Pessah IN. Divergent functional properties of ryanodine receptor types 1 and 3 expressed in a myogenic cell line. Biophys J. 2000; 79:2509–2525. [PubMed: 11053126]

Fill M, Copello JA. Ryanodine receptor calcium release channels. Physiol Rev. 2002; 82:893–922. [PubMed: 12270947]

Franzini-Armstrong C, Jorgensen AO. Structure and development of E–C coupling units in skeletal muscle. Annu Rev Physiol. 1994; 56:509–534. [PubMed: 8010750]

Futatsugi A, Kato K, Ogura H, Li ST, Nagata E, Kuwajima G, Tanaka K, Itohara S, Mikoshiba K. Facilitation of NMDAR-independent LTP and spatial learning in mutant mice lacking ryanodine receptor type 3. Neuron. 1999; 24:701–713. [PubMed: 10595520]

Giannini G, Conti A, Mammarella S, Scrobogna M, Sorrentino V. The ryanodine receptor/calcium channel genes are widely and differentially expressed in murine brain and peripheral tissues. J Cell Biol. 1995; 128:893–904. [PubMed: 7876312]

Hanson MG, Fregoso VL, Vrana JD, Tucker CL, Niswander LA. Peripheral nervous system defects in a mouse model for peroxisomal biogenesis disorders. Dev Biol. 2014; 395:84–95. [PubMed: 25176044]

Hanson MG, Landmesser LT. Normal patterns of spontaneous activity are required for correct motor axon guidance and the expression of specific guidance molecules. Neuron. 2004; 43:687–701. [PubMed: 15339650]

Hanson MG, Landmesser LT. Increasing the frequency of spontaneous rhythmic activity disrupts pool-specific axon fasciculation and pathfinding of embryonic spinal motoneurons. J Neurosci. 2006; 26:12769–12780. [PubMed: 17151280]

Hanson MG, Niswander LA. An explant muscle model to examine the refinement of the synaptic landscape. J Neurosci Methods. 2014; 238:95–104. [PubMed: 25251554]

Hanson MG, Wilde JJ, Moreno RL, Minic AD, Niswander L. Potassium dependent rescue of a myopathy with core-like structures in mouse. Elife. 2015:4.

Kasarskis A, Manova K, Anderson KV. A phenotype-based screen for embryonic lethal mutations in the mouse. Proc Natl Acad Sci USA. 1998; 95:7485–7490. [PubMed: 9636176]

Kim N, Burden SJ. MuSK controls where motor axons grow and form synapses. Nat Neurosci. 2008; 11:19–27. [PubMed: 18084289]

Kim N, Stiegler AL, Cameron TO, Hallock PT, Gomez AM, Huang JH, Hubbard SR, Dustin ML, Burden SJ. Lrp4 is a receptor for Agrin and forms a complex with MuSK. Cell. 2008; 135:334–342. [PubMed: 18848351]

Kinoshita SM, Kogure A, Taguchi S, Nolan GP. Snapin, positive regulator of stimulation- induced Ca(2)(+) release through RyR, is necessary for HIV-1 replication in T cells. PLoS One. 2013; 8:e75297. [PubMed: 24130701]

Krull CE. Neural crest cells and motor axons in avians: common and distinct migratory molecules. Cell Adhes Migr. 2010; 4:631–634.

Levitan ES. Signaling for vesicle mobilization and synaptic plasticity. Mol Neurobiol. 2008; 37:39–43. [PubMed: 18446451]

Lin W, Burgess RW, Dominguez B, Pfaff SL, Sanes JR, Lee KF. Distinct roles of nerve and muscle in postsynaptic differentiation of the neuromuscular synapse. Nature. 2001; 410:1057–1064. [PubMed: 11323662]

Magill-Solc C, McMahan UJ. Motor neurons contain agrin-like molecules. J Cell Biol. 1988; 107:1825–1833. [PubMed: 2846587]

Misgeld T, Kummer TT, Lichtman JW, Sanes JR. Agrin promotes synaptic differentiation by counteracting an inhibitory effect of neurotransmitter. Proc Natl Acad Sci USA. 2005; 102:11088–11093. [PubMed: 16043708]

Nakai J, Imagawa T, Hakamat Y, Shigekawa M, Takeshima H, Numa S. Primary structure and functional expression from cDNA of the cardiac ryanodine receptor/calcium release channel. FEBS Lett. 1990; 271:169–177. [PubMed: 2226801]

Nelson BR, Wu F, Liu Y, Anderson DM, McAnally J, Lin W, Cannon SC, Bassel-Duby R, Olson EN. Skeletal muscle-specific T-tubule protein STAC3 mediates voltage-induced Ca^{2+} release and contractility. Proc Natl Acad Sci USA. 2013; 110:11881–11886. [PubMed: 23818578]

Numa S, Tanabe T, Takeshima H, Mikami A, Niidome T, Nishimura S, Adams BA, Beam KG. Molecular insights into excitation–contraction coupling. Cold Spring Harb Symp Quant Biol. 1990; 55:1–7. [PubMed: 1966760]

Otsu K, Willard HF, Khanna VK, Zorzato F, Green NM, MacLennan DH. Molecular cloning of cDNA encoding the Ca^{2+} release channel (ryanodine receptor) of rabbit cardiac muscle sarcoplasmic reticulum. J Biol Chem. 1990; 265:13472–13483. [PubMed: 2380170]

Plomp JJ, van Kempen GT, Molenaar PC. Adaptation of quantal content to decreased postsynaptic sensitivity at single endplates in alpha-bungarotoxin-treated rats. J Physiol. 1992; 458:487–499. [PubMed: 1302275]

Powell JA, Rieger F, Blondet B, Dreyfus P, Pincon-Raymond M. Distribution and quantification of ACh receptors and innervation in diaphragm muscle of normal and mdg mouse embryos. Dev Biol. 1984; 101:168–180. [PubMed: 6692971]

Reist NE, Werle MJ, McMahan UJ. Agrin released by motor neurons induces the aggregation of acetylcholine receptors at neuromuscular junctions. Neuron. 1992; 8:865–868. [PubMed: 1316763]

Rimer M. Modulation of agrin-induced acetylcholine receptor clustering by extracellular signal-regulated kinases 1 and 2 in cultured myotubes. J Biol Chem. 2010; 285:32370–32377. [PubMed: 20696763]

Sanes JR, Lichtman JW. Development of the vertebrate neuromuscular junction. Annu Rev Neurosci. 1999; 22:389–442. [PubMed: 10202544]

Sanes JR, Lichtman JW. Induction, assembly, maturation and maintenance of a postsynaptic apparatus. Nat Rev Neurosci. 2001; 2:791–805. [PubMed: 11715056]

Shakiryanova D, Klose MK, Zhou Y, Gu T, Deitcher DL, Atwood HL, Hewes RS, Levitan ES. Presynaptic ryanodine receptor-activated calmodulin kinase II increases vesicle mobility and potentiates neuropeptide release. J Neurosci. 2007; 27:7799–7806. [PubMed: 17634373]

Takeshima H, Iino M, Takekura H, Nishi M, Kuno J, Minowa O, Takano H, Noda T. Excitation–contraction uncoupling and muscular degeneration in mice lacking functional skeletal muscle ryanodine-receptor gene. Nature. 1994; 369:556–559. [PubMed: 7515481]

Takeshima H, Ikemoto T, Nishi M, Nishiyama N, Shimuta M, Sugitani Y, Kuno J, Saito I, Saito H, Endo M, Iino M, Noda T. Generation and characterization of mutant mice lacking ryanodine receptor type 3. J Biol Chem. 1996; 271:19649–19652. [PubMed: 8702664]

Takeshima H, Komazaki S, Hirose K, Nishi M, Noda T, Iino M. Embryonic lethality and abnormal cardiac myocytes in mice lacking ryanodine receptor type 2. EMBO J. 1998; 17:3309–3316. [PubMed: 9628868]

Takeshima H, Nishimura S, Matsumoto T, Ishida H, Kangawa K, Minamino N, Matsuo H, Ueda M, Hanaoka M, Hirose T, Numa S. Primary structure and expression from complementary DNA of skeletal muscle ryanodine receptor. Nature. 1989; 339:439–445. [PubMed: 2725677]

Wang JY, Chen F, Fu XQ, Ding CS, Zhou L, Zhang XH, Luo ZG. Caspase-3 cleavage of dishevelled induces elimination of postsynaptic structures. Dev Cell. 2014; 28:670–684. [PubMed: 24631402]

Weatherbee SD, Anderson KV, Niswander LA. LDL-receptor-related protein 4 is crucial for formation of the neuromuscular junction. Development. 2006; 133:4993–5000. [PubMed: 17119023]

Yang X, Arber S, William C, Li L, Tanabe Y, Jessell TM, Birchmeier C, Burden SJ. Patterning of muscle acetylcholine receptor gene expression in the absence of motor innervation. Neuron. 2001; 30:399–410. [PubMed: 11395002]

Zissimopoulos S, West DJ, Williams AJ, Lai FA. Ryanodine receptor interaction with the SNARE-associated protein snapin. J Cell Sci. 2006; 119:2386–2397. [PubMed: 16723744]

Zorzato F, Fujii J, Otsu K, Phillips M, Green NM, Lai FA, Meissner G, MacLennan DH. Molecular cloning of cDNA encoding human and rabbit forms of the Ca^{2+} release channel (ryanodine receptor) of skeletal muscle sarcoplasmic reticulum. J Biol Chem. 1990; 265:2244–2256. [PubMed: 2298749]

Appendix A. Supplementary material

Supplementary data associated with this article can be found in the online version at http://dx.doi.org/10.1016/j.ydbio.2015.05.018

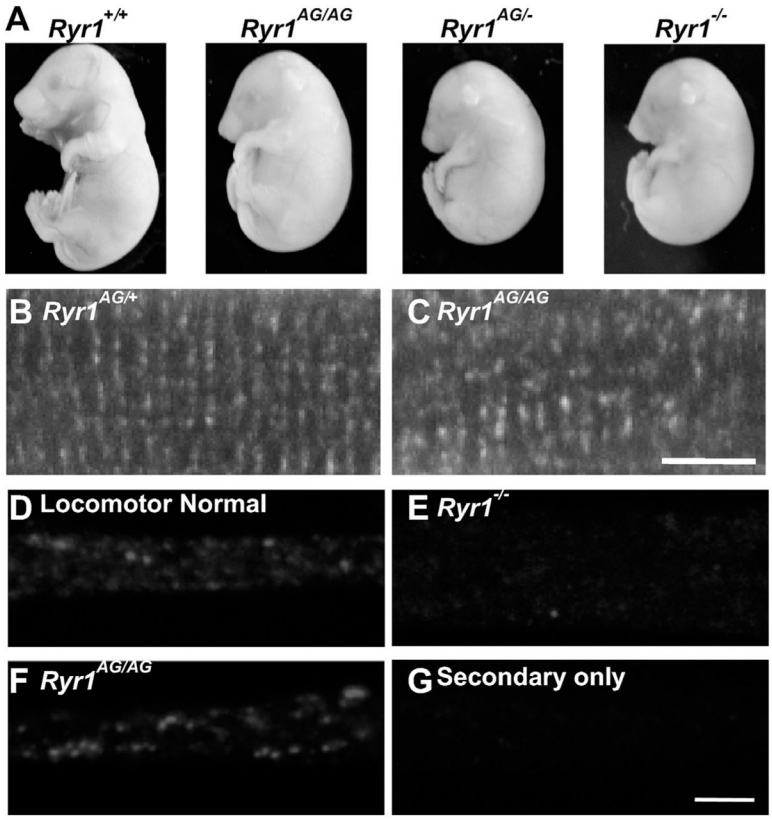

Fig. 1.

ENU-induced mutation in *Ryr1*. (A) Complementation cross of $Ryr1^{AG/+}$ with $Ryr1^{-/+}$ results in trans-heterozygous embryos with the same gross phenotype as $Ryr1^{AG/AG}$ mutants and $Ryr1^{-/-}$ nulls. (B, C) Immunohistochemistry of muscle fibers labeled with pan-RyR antibody. (D–G) Punctate immunostaining was observed in normal (D) and $Ryr1^{AG/AG}$ (E) myotubes, but not in $Ryr1^{-/-}$ myotubes (F). Staining was absent when only the secondary antibody was present.

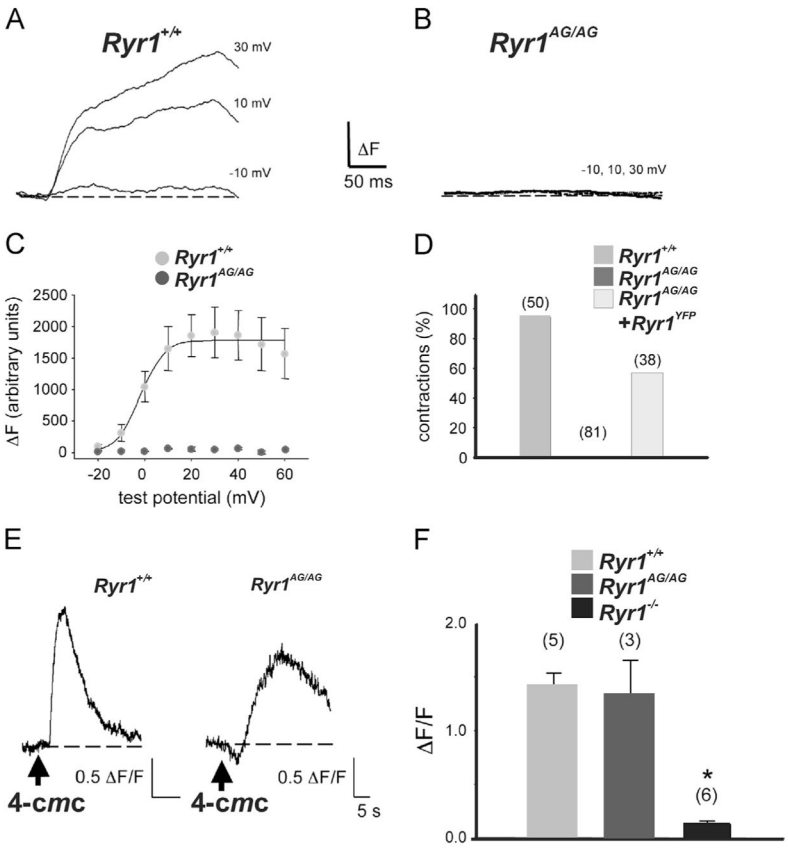

Fig. 2.

Ryr1$^{AG/AG}$ show defects in calcium dynamics. (A, B) Representative recordings of myoplasmic Ca^{2+} transients elicited by 50-ms depolarizations from −50 mV to the indicated test potentials for locomotor normal myotubes (A; *Ryr1*$^{+/+}$) and *Ryr1*$^{AG/AG}$ myotubes (B). (C) Comparison of Δ*F*−*V* relationships for normal myotubes (light gray circles; *n*=4), and *Ryr1*$^{AG/AG}$ myotubes (dark gray circles; *n*=7). (D) Fraction of myotubes that contract in response to a 100 V, 10 ms electrical stimulus for normal myotubes (light gray bar), *Ryr1*$^{AG/AG}$ myotubes (dark gray bar, 0%), and *Ryr1*$^{AG/AG}$ myotubes transfected with RyR1-YFP (white bar). (E) Representative changes in Fluo-3 AM fluorescence in response to application of 4-chloro-*m*-cresol (4-C*m*C; 0.5 mM) elicited in a normal myotube (left) and *Ryr1*$^{AG/AG}$ myotube (right). Arrows indicate time of 4-C*m*C applications. (F) Half-rise times of Ca^{2+} transients in response to 4-C*m*C for normal (light gray bar), and *Ryr1*$^{AG/AG}$ (dark gray bar) myotubes compared to *Ryr1*$^{-/-}$ (black bar). Error bars represent ± SEM. Asterisks indicate a significant difference (*p*=0.006; *t*-test). For each group in (D) and (F), the total number of myotubes tested is indicated above each bar.

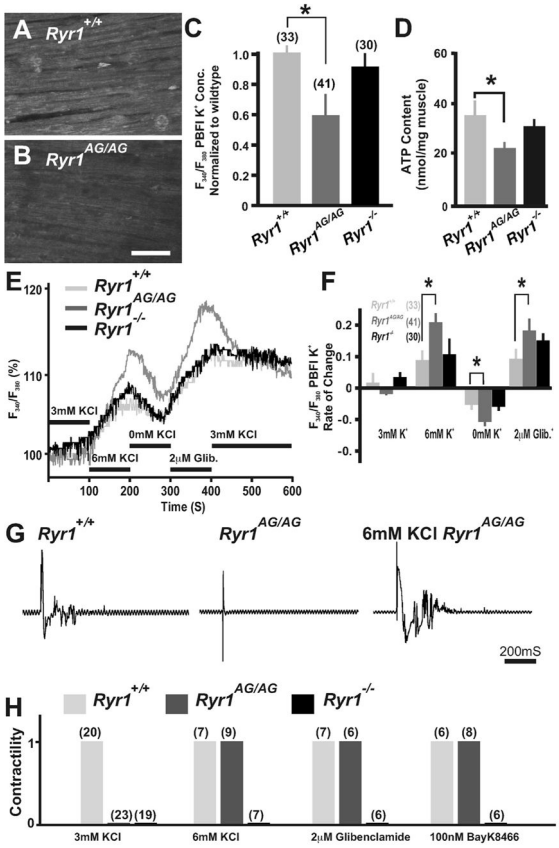

Fig. 3.

Ryr1$^{AG/AG}$ muscle regains contractility with masked potassium leak. (A, B) Fluorescence imaging of PBFI at 340 nm in *Ryr1*$^{+/+}$ (A) and *Ryr1*$^{AG/AG}$ (B) diaphragm in 3 mM Ringers solutions. Scale bar=50 μM. (C) Ratiometric potassium imaging obtained at 340 and 380 nm wavelengths provided a ratio of fluorescence in *Ryr1*$^{+/+}$ (light gray), *Ryr1*$^{AG/AG}$ (dark gray) and *Ryr1*$^{-/-}$ (black) diaphragm muscle (normalized to *Ryr1*$^{+/+}$). (D) ATP determination of E18.5 muscles. (E) Representation of the ratiometric imaging experimental paradigms for *Ryr1*$^{+/+}$ (light gray), *Ryr1*$^{AG/AG}$ (dark gray) and *Ryr1*$^{-/-}$ (black) diaphragm muscle with bath applications of 3 mM KCl, 7 mM KCl, 0 mM KCl and 3 mM KCl with 2 μM glibenclamide in Ringers solutions. (F) Change of intracellular K^+ fluorescence intensities in experimental conditions. (G) EMG recordings of diaphragm muscle from *Ryr1*$^{+/+}$, *Ryr1*$^{AG/AG}$, or *Ryr1*$^{AG/AG}$ treated with 6 mM KCl. (H) Analysis of contractility of E18.5 diaphragm muscle from *Ryr1*$^{+/+}$, *Ryr1*$^{AG/AG}$, or *RyR1*$^{-/-}$ embryos. After equilibration, all samples were bathed first in 6 mM KCl, followed by wash out and then addition of one of the following conditions as indicated (3 and 6 mM KCl, 2 μM glibenclamide and 100 nM Bay K8644; *n* for experiments above bars).

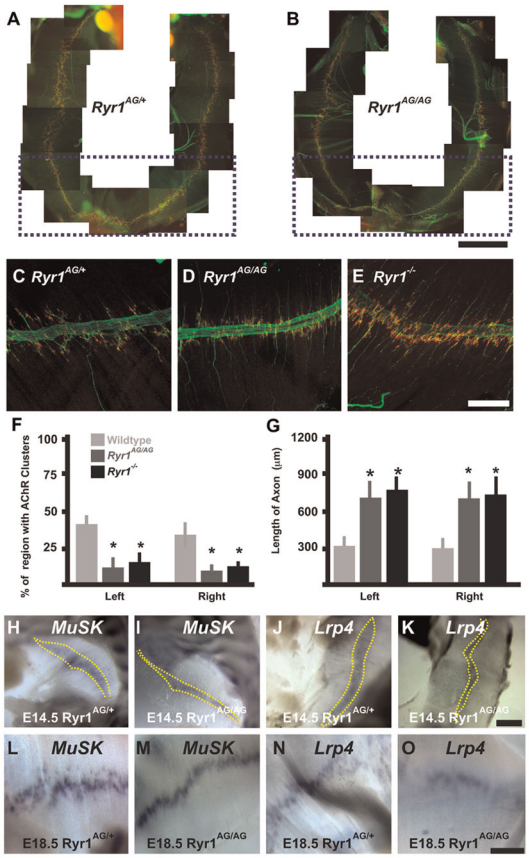

Fig. 4.

Narrowed AChR cluster distribution and increased motor axon outgrowth in *Ryr1*$^{AG/AG}$diaphragms. (A, B) E18.5 whole diaphragms show clustered AChRs that form neuromuscular junctions visualized with α–bungarotoxin (red) and axons with synaptophysin and neurofilament (green; scale bar in A, B=1 mm). (C–E) Left ventral quadrants of diaphragms (scale bar=200 µm). (C) In *Ryr1*$^{AG/+}$ diaphragms, AChR clusters extend along the axon branches. (D, E) In *Ryr1*$^{AG/+}$ and *Ryr1*$^{-/-}$ diaphragms, AChR clusters surround the fasciculated nerve but do not extend along the axon branch. (F–G) Quantification in the ventral quadrant (outlined by purple boxes in A, B) of AChR cluster regionalization (F) and axon length (G) (*n*=5 for each). H–O, At 14.5 (H–K, scale bar=100 µm) and at E18.5 (L–O, scale bar=200 µm), *MuSK* and *Lrp4* (yellow dashes) are expressed in the central region of *Ryr1*$^{AG/+}$ and *Ryr1*$^{AG/AG}$ diaphragms.

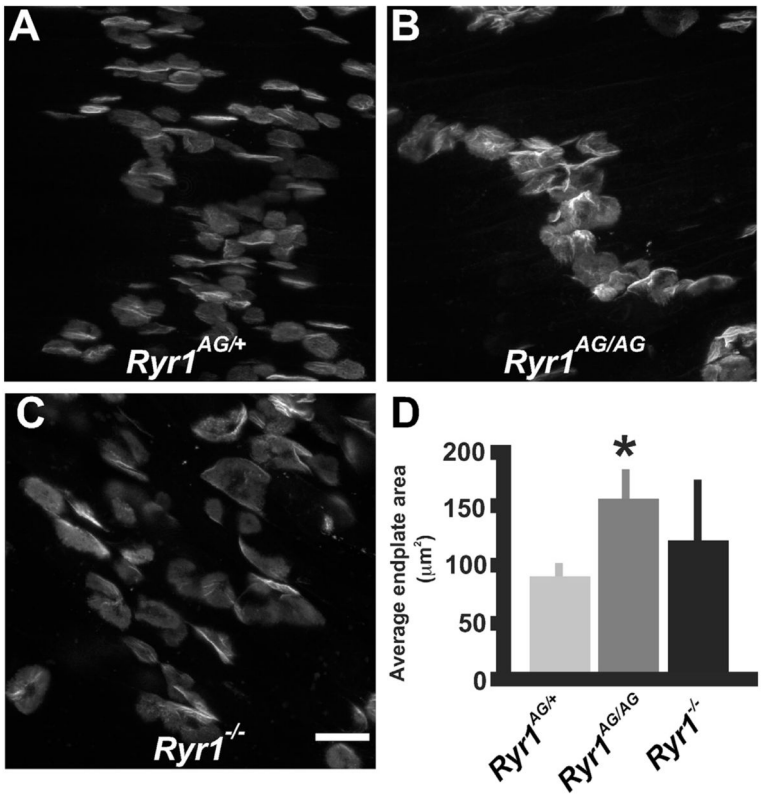

Fig. 5.

RYR1 controls AChR cluster size. (A–C) AChR clusters of *Ryr1*$^{AG/+}$, *Ryr1*$^{AG/AG}$, and *Ryr1*$^{-/-}$ endplates (scale bar=20 μm). (D) Quantification in the ventral quadrant of the diaphragm of AChR cluster size.

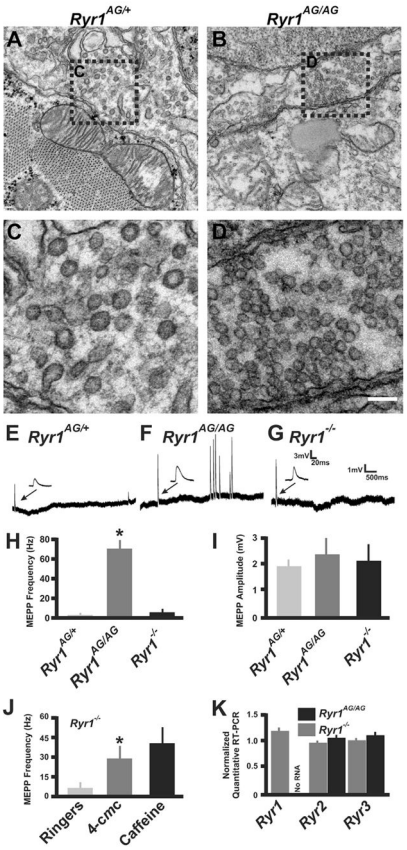

Fig. 6.

Ryr1$^{AG/AG}$ embryos show increased synaptic vesicles and miniature endplate potentials. (A–D) Transmission EM of E18.5 phrenic nerve terminals and synaptic vesicles in *Ryr1*$^{AG/AG}$ (A, C) compared to *Ryr1*$^{AG/+}$ (B, D). A, B Scale bar=500 nm. (C and D) magnified view of boxed regions in A, B. (E–G) Recordings of spontaneous events demonstrate increased frequency of mEPPs in *Ryr1*$^{AG/AG}$ (F) compared to *Ryr1*$^{AG/+}$ (E) and *Ryr1*$^{-/-}$ (G). (H) Quantification of mEPP frequency. (I) Quantification of mEPP amplitude. (J) Examination of mEPPs per minute after application of either 500 μM 4-C*m*C or 1 μM caffeine in *Ryr1*$^{-/-}$ diaphragm. (K) Quantitative RT-PCR of *Ryr1*, *Ryr2* and *Ryr3* from the ventral spinal cord of *Ryr1*$^{+/+}$, *Ryr1*$^{AG/AG}$, *Ryr1*$^{-/-}$ embryos (*n*=4 each) and the data normalized to the level of expression in wild type.

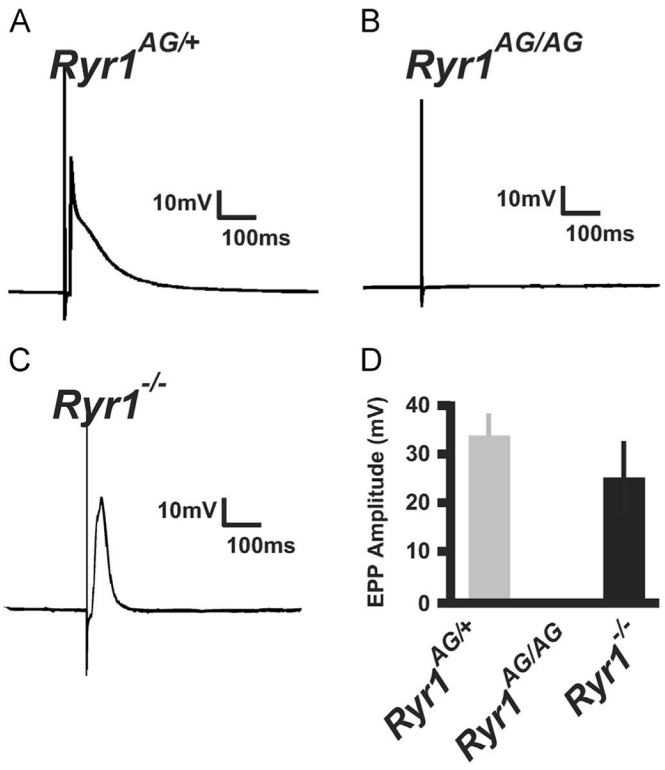

Fig. 7.

Lack of evoked endplate potentials in RyR1$^{AG/AG}$ muscle. Sharp electrode recordings of responses from diaphragm muscle following a 0.2 ms suprathreshold stimulus to the phrenic nerve in normal Ringer's solution. (A–C) Representative recording of evoked response in *Ryr1*$^{AG/+}$ (A) and *Ryr1*$^{-/-}$(C) compared to complete lack of evoked response in *Ryr1*$^{AG/AG}$ (B). (D) Quantification of evoked end-plate potentials from *Ryr1*$^{AG/+}$, *Ryr1*$^{AG/AG}$ and *Ryr1*$^{-/-}$ diaphragms.

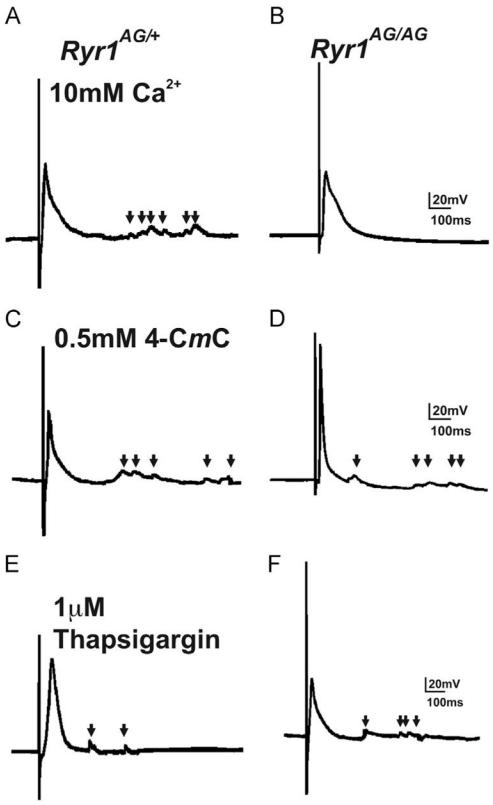

Fig. 8.

Rescue of evoked EPP in *Ryr1*$^{AG/AG}$ muscle. Resumption of evoked EPPs in *Ryr1*$^{AG/AG}$ by application of 10 mM Ca^{2+} (B), 500 μM 4-C*m*C (D), or 1 μM thapsigargin (F) compared to *Ryr1*$^{AG/+}$ (A, C and E). Arrows represent mEPPs.